GPR applications in structural detailing of a major tunnel using different frequency antenna systems

GPR Applications in Structural Detailing of a Major Tunnel Using Different Frequency Antenna Systems

Amir M. ALANI and Fabio TOSTI

School of Computing and Engineering, University of West London (UWL), St Mary's Road, Ealing, London W5 5RF, UK

Amir.Alani@uwl.ac.uk; Fabio.Tosti@uwl.ac.uk

Abstract

This paper reports an extended study on the applications of ground penetrating radar (GPR) on the structural detailing of a major tunnel located under the River Medway in north Kent, United Kingdom (the Medway Tunnel). Construction of the tunnel was completed in 1996 and it carries a substantial volume of traffic between two major areas of Medway in the south east of England. The construction of the tunnel is an "immersed tube" tunnel type that connects a number of segments at immersion joint points. This investigation reports the utilisation of two sets of antenna systems with different frequencies (900MHz and 2GHz GPR) in establishing structural details of the tunnel roof at immersion joints. The processed data compiled as a result of this investigation provided essential information to tunnel engineers for forthcoming maintenance planning purposes. The data also provided ample information confirming rather doubted construction design drawings/plans originally produced. The results obtained were conclusive in terms of construction materials and structural design configurations (shape and dimensions) as well as the identification of rebar positions at all three immersion joint locations. A comparison between the different frequency antenna sets provided invaluable information in confirming the above findings. This paper also provides useful information

within the context of survey planning and site procedure in a complex operation in terms of adaptation of the GPR systems used.

Keywords: Tunnel lining; Health monitoring and assessment; Ground Penetrating Radar (GPR); Data interpretation

1. Introduction

Tunnels are one of the most important infrastructural assets and are crucial to human life in mobility, financial and environmental terms. They are built for rails, roads, passages, sewage, water and utilities. Various processes may cause damage to tunnel structural integrity and failures can broadly be divided into two main classes: those occurring during construction and those happening after a structure has been put into service. With regards to the first category, one of the major causes of failure is related to the ground settlement when tunnelling, especially in case of soft grounds [1]. The effects induced by the ageing process over time and physical agents such as water ingress are among the main causes of ongoing problems during the working life of a tunnel, sometimes affecting not only the tunnel lining but also the structures and fittings within the tunnel. According to a report from the International Tunnelling and Underground Space Association (ITA) [2], the damaging effects of water on tunnels during their working life may be classified by three main classes: i) external effects (not affecting the structure and acting on the surroundings of the tunnel), ii) structural effects (with implications on the structural adequacy of the tunnel) and iii) functional effects (affecting the functionality of the tunnel). Deterioration of mortar, corrosion of reinforcement due to the electrolytic action brought about by the chloride contamination of the concrete, degradation and reduction in the strength of concrete, and the erosion of mortar in the masonry lining are amongst the main problems identified in historical cases.

The implementation of a robust tunnel health monitoring, in terms of structural assessment and maintenance, must be considered as a crucial element in limiting and preventing the degradation of these structures as well as in performing reliable worst case fire safety risk assessments, with paramount importance in case of emergency situations. In addition, a lot of information in construction design drawings needs to be verified, as it frequently deals with very poorly vibrated concrete, incorrectly positioned reinforcement bars or untrue thickness of covering concrete with respect to the information included in original design plans [3, 4].

Depending on the type and requirements of a tunnel, different approaches should be adopted to acquire relevant and useful information. Different types of non-destructive testing (NDT) techniques are available within the context of tunnel health monitoring. Among the most acknowledged and established acoustic methods, the ultrasonic tomography (UST) and the impact echo (IE) are worthy of mention, whereas ground penetrating radar (GPR) is one of the most used electromagnetic methods [5-7]. Overall, no NDT technique has proved to be self-reliant and capable of producing comprehensive information in terms of tunnel condition surveys, though they all have found positive findings for certain applications.

In this framework, the use of GPR in the monitoring and assessment of critical highway infrastructures such as bridges and tunnels has found the first relevant literature evidence in the 2000s [8-10], and it has gained momentum in recent years [11-13]. The work reported by Li et al. [14] presented new developing approaches in the applications of GPR in tunnel lining assessment. In this study, the authors introduce the peak value criterion method which was employed to recognise the lining interfaces of tunnels. The combination of GPR and finite-difference time-domain (FDTD) techniques based on prior information about the designed tunnel structure is also emerging as an effective approach in assisting the interpretation of the data collected on the site [15, 16]. The utilisation of GPR in conjunction with other non-destructive and non-contact testing methods has also been introduced in the assessment and

monitoring of highway infrastructures [17, 18]. In general, GPR is now established as one of the most acknowledged NDTs with a multi-task utilisation and high productivity granted by the various available configurations of the systems and central frequencies of investigation that can be selected according to the specific purposes of the investigation.

This paper provides a detailed account of the project planning, the survey method adopted and the survey performance carried out on a major tunnel located in the south east of the United Kingdom. Particular attention has been paid in given to reporting the challenges encountered during the actual survey and the outcomes arising from the utilisation of two different sets of frequency GPR antennas.

The paper first addresses the aim and objectives of the study. The theoretical background is then discussed, by providing insights on GPR principles, operating frequencies and processing techniques for wave velocity estimation in tunnelling applications. The case study is then introduced and details of equipment, survey methodology, data acquisition and processing are subsequently defined. Results and discussion of the main findings concerning two expansion joints are addressed and the conclusion and future prospects are finally drawn.

2. Aim and objectives

The main aim of the investigation reported in this paper is to verify the effectiveness of GPR in gaining vital information about the design configuration of an immersed tube tunnel at several immersion joint locations, by using different central frequencies of investigation. This is a contribution to the research for performing effective and reliable worst case fire safety risk assessments, i.e., the evaluation of time before the structural collapse of tunnel joints in case of burning vehicles containing fuel and additional combustible materials. To that effect, attention was given to the understanding of the exact construction details of the joints as well

as to checking the consistency between information retrieved by GPR and information available by design drawings.

The main aim of the investigation was achieved by the following set objectives:

- exact location of immersion joints (the approximate joint location was known);
- thickness of covering concrete at joints;
- depth and location of reinforcement (rebar);
- identification of depth and presence of the Rockwool Rollbatts (i.e., special protective material made of mineral wood and used as cover for the Omega Seal);
- identification of the position of the Omega Seals, if possible.

3. Theoretical background

3.1.GPR principles

GPR is a geophysical inspection technique that uses a transmitter to emit a pulse of electromagnetic (EM) energy into the subsurface and receives the back-reflected energy. The electric and magnetic properties of the medium passed through rule the propagation of the EM wave. These are identified as dielectric permittivity ε and electric conductivity σ, in terms of electric properties, and magnetic permeability μ as the magnetic property. The behaviour of the propagating wave is greatly influenced by ε and σ in terms of wave velocity and wave attenuation, respectively. On the contrary, μ does not affect the propagation of the EM wave, and it is equal to the free space magnetic permeability μ_0 for all the non-magnetic materials. A dielectric contrast in a medium causes a partial reflection and transmission of the EM impulse. As a function of the operating mode, the reflected or transmitted part of a signal is collected by the receiving antenna. The strength of the reflections and the corresponding receiving time are then recorded by the receiver and finally displayed. In structural monitoring applications of tunnel roofs, GPR is used to send an ultra-high frequency EM impulse into the tunnel lining.

When discontinuities in the dielectric properties of the lining are encountered (e.g., rebars, interfaces between different materials, voids, cracks or fissures) the wave gets reflected and it is recorded by the receiver through the receiving antenna. Penetration depth and vertical resolution are influenced by several factors, amongst which the frequency of the emitted signal and the type and physical condition of the material investigated are worth mentioning. In this regard, several pieces of research on how to retrieve physical and geometrical information related to transport infrastructures and foundation soils from the frequency information and the electric properties of the collected signal (e.g., moisture of subgrade soils [19] and thickness of road pavement layers [20] from spectral analyses of the GPR signal and inversion algorithms) can be found in the literature.

3.2.The GPR operating frequency

The EM waves are characterized by the frequency at which they oscillate, and the engineering trade-off between the operating frequency and the signal resolution is one of the major challenges to tackle for a GPR operator. Low-frequency antennas produce longer wavelengths and higher frequency antennas generate shorter wavelengths, according to the following equation:

$$\lambda_c = \frac{v}{f_c} \tag{1}$$

Here, λ_c is the central frequency wavelength, v is the velocity of the propagating wave in the medium and f_c is the central frequency. Thereby, high-frequency signals in low-velocity media are characterized by the shortest wavelength and the highest resolution. Accordingly, the lowest resolution is reached in the case of a low-frequency signal in a high-velocity medium.

On the other hand, the attenuation of a GPR signal is strongly controlled by and proportional to the frequency, whereas the velocity is not so dependent on frequency [21]. Higher frequencies attenuate significantly more than low frequencies, and a relative loss of the high-

frequency signal component occurs as the wave propagates, especially in cases of damp/wet subsurface materials. This frequency-dependent behaviour of the attenuation also explains the highest penetration of lower-frequency GPR signals than higher frequencies. Overall, longer waves penetrate deeper in the medium but shorter waves offer a better resolution.

As a rule of thumb, given a maximum target depth it is recommended to select the highest frequency antenna capable of penetrating to that depth, in order to provide the best trade-off between desirable resolution and desirable depth of penetration.

3.3.Velocity estimation by hyperbola fitting

Determining the velocity of wave propagation in a medium can be accomplished through several methods [22]. One of the most frequently used methods in tunnel engineering is the hyperbola fitting, due to the presence of buried localised reflectors (e.g., immersion joints), or buried cylindrical-shaped objects (e.g., rebar layer, pipes). Among the factors that influence the shapes of these hyperbolae we can mention the nature of the subsurface reflector, the relative permittivity of the medium in which the objects are located, as well as the physical conditions of both these materials.

Assuming transmitting and receiving antennas in the same position (i.e., monostatic configuration), homogeneity of the subsurface medium and isotropy of the cylindrical-shaped targets, we can assume the wave propagation velocity as constant in the hyperbolic mathematical model of buried cylindrical objects [23]. Fig. 1(a) shows the model of a hyperbola generated by a buried cylindrical-shaped object of radius R with the GPR antenna moving on the surface along the x-axis (i.e., the scanning direction), and being v the velocity of wave propagation in the medium. Three reference positions of the GPR antenna, namely, x_i (abscissa of the initial point of the first arm of the generated hyperbola), x_0 (abscissa of the hyperbola apex), and x_f (abscissa of the final point of the descending arm of the hyperbola)

define the hyperbola shape, being z_i, z_0, and z_f being the corresponding distances to the cylinder surface with two-way travel times of t_i, t_0, and t_f, respectively.

According to Fig. 1(a) and computing with the Pythagoras' theorem, the following relationship can be written:

$$(z_i + R^2) = (z_0 + R^2) + (x - x_0) \tag{2}$$

Substituting z_i with $v \times t_i/2$ and z_0 with $v \times t_0/2$ in Eq. (2), the hyperbolic equation can be written as follows:

$$\frac{(t_i+2R/v)^2}{(t_0+2R/v)^2} - \frac{(x_i-x_0)^2}{(vt_0/2+R)^2} = 1 \tag{3}$$

This represents the equation of a hyperbola centered around (z_0; - $2R/v$). From Eq. (3), the hyperbola semi-axes a and b (Fig. 1(b)) are given by:

$$a = t_0 + 2Rv \tag{4}$$

$$b = \frac{v}{2}t_0 + R = \frac{v}{2}a \tag{5}$$

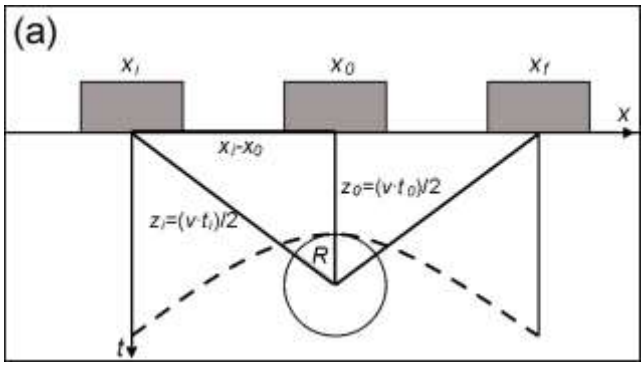

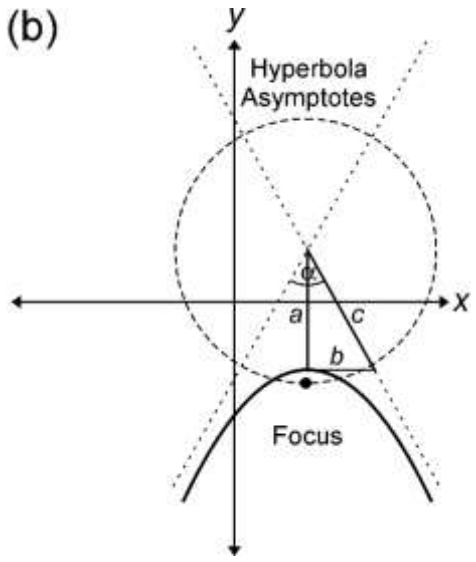

Fig. 1. (a) Diagram of the reflection hyperbola generated by a cylindrical object of radius *R*, (b) general hyperbola with asymptotes and equation parameters.

The angle α between the hyperbola asymptotes is defined using Eq. (4) and Eq. (5) as follows:

$$tg\ \alpha = \frac{b}{a} = \frac{v}{2} \tag{6}$$

It can be seen from Eq. (6) that the angle α is directly proportional to v. Hence, if the same value of R is kept, then increasing values of v correspond to increasing values of α, and vice versa. The wave velocity v can be therefore written as:

$$v = 2\ tg\ \alpha = 2\ \frac{b}{a} = \tag{7}$$

where v is a function of the vertex coordinates, the object radius and the time delay. Several models have been proposed in the literature about the estimation of these parameters in GPR hyperbola reflections [24-27], and the error expected when the center position of the hyperbola is not identified properly or when the radius of the reflecting object changes [28]. In this paper, velocity estimation was obtained from the slope of the hyperbola (i.e., angle α) after manually fitting its shape [29]. The velocity is therefore used to estimate the depth D to the desired reflector/interface according to the following equation:

$$D = \frac{v\ t_0}{2} = \frac{b\ t_0}{a} \tag{8}$$

where v is the wave velocity of propagation in the medium and t_0 is the two-way travel time delay of the reflector/interface (at the apex abscissa) from the surface, respectively.

4. Case study: the Medway Tunnel

The Medway Tunnel is a tunnel located under the River Medway, linking Strood with Chatham in Kent, England (Fig. 2). The tunnel was opened to the public in June 1996. It comprises of a link road approximately 1500m in length, 720 m of which is within the tunnel under the River Medway.

Fig. 2. Medway Tunnel eastbound entrance.

The Medway Tunnel was the first immersed tube tunnel to be built in England. It was built in three distinct sections. The central part of the tunnel comprises 370 m of immersed tube, which is linked to cut and cover tunnels on both the east and west banks of the river. Three immersed tube sections were built with dimensions of 23.9 m wide and 9.15 m high, with one section measuring 118 m and the other two 126 m in length (Fig. 3).

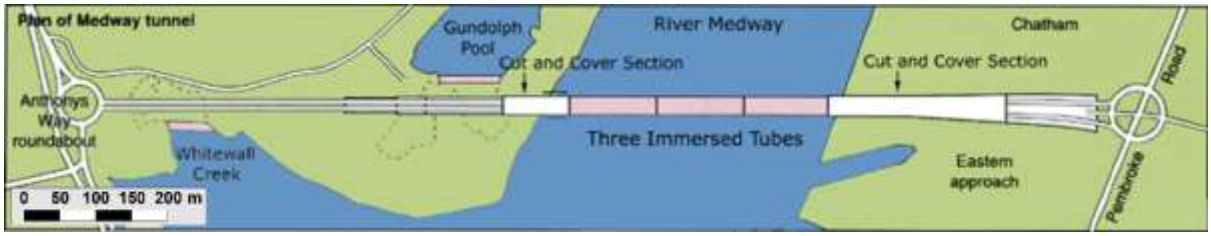

Fig. 3. Depiction of the three immersion tube sections of the tunnel.

With regard to the available design drawings of structural details, Fig. 4(a-b) depicts the immersion joints complemented by a simplified reproduction drawing. The key points of the construction can be summarised as:

- a rubber seal (Omega Seal) forms the watertight joint between the tunnel sections;
- below this seal is a layer of Rockwool Rollbatts (insulation) material;
- the Rockwool Rollbatts are covered by a shotcrete layer of 250 mm approximately.

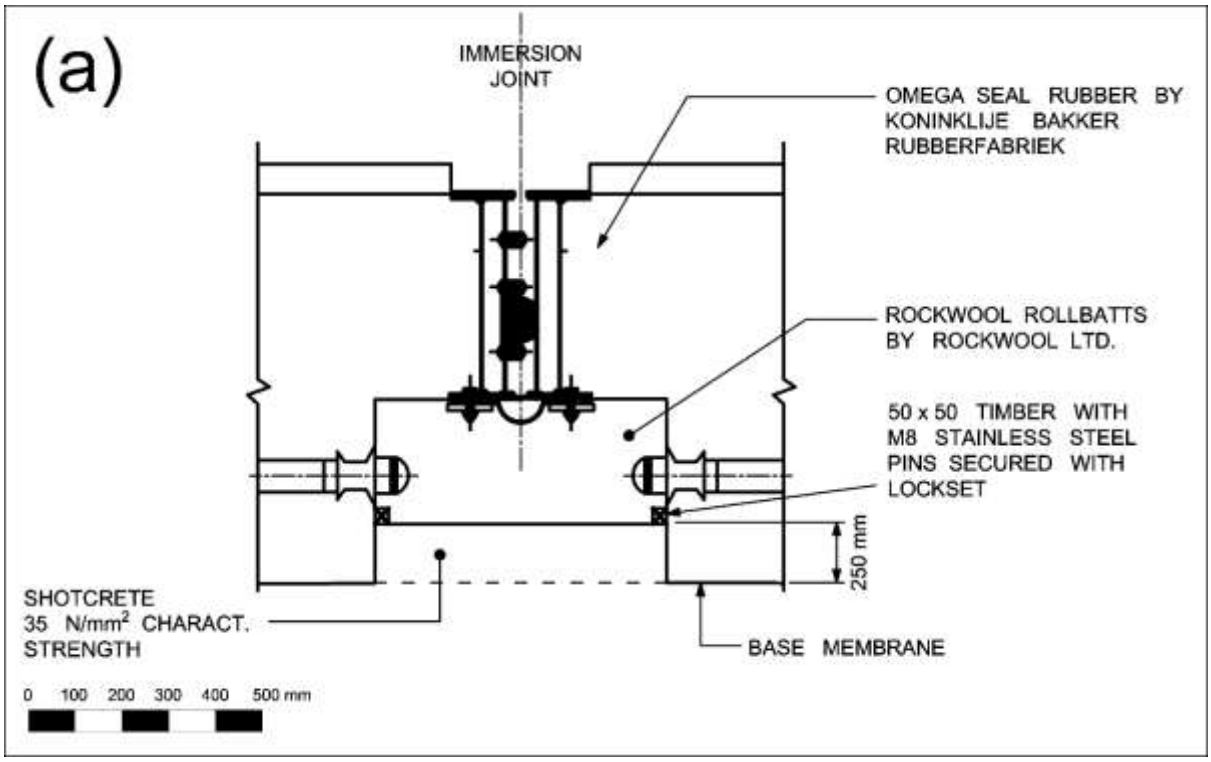

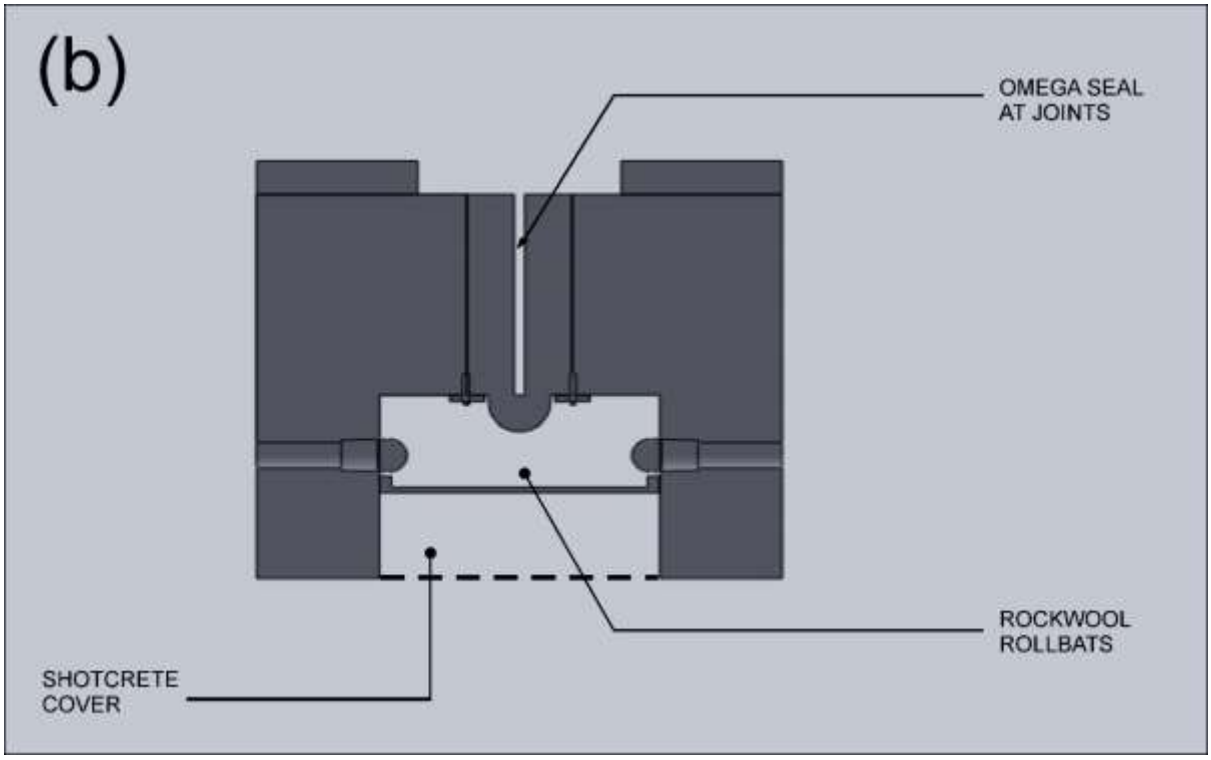

Fig. 4. Cross-section of roof immersion joints (a) original design drawing, (b) simplified drawing.

5. Equipment

Two GPR systems manufactured by IDS Georadar were used to materialise the above set objectives. The RIS MF Hi-Mod multi-frequency system, set with 400 MHz and 900 MHz antennas, was used. For the purposes of this study, only the data collected with the 900 MHz antenna were processed and analysed. In addition, the hand-held RIS FastWave GPR system, TR-HF 2 GHz antenna was used to collect high resolution data. The selection of these systems was carried out in compliance to the requirements of the survey. Indeed, details of joint construction and thickness estimation of the construction elements needed to be ascertained with high precision. To that effect, nominal resolutions of 8.33 cm and 3.75 cm (quarter of wavelength criterion) can be obtained with the 900 MHz and the 2 GHz systems, respectively.

6. Survey Methodology

This study focuses on the structural details of joints “B” and “C” of the Medway Tunnel. Comparisons of the results with relevant outcomes achieved by Alani and Banks [4] within the structural detailing of joint “A” are also addressed. A 900 MHz GPR survey at immersion joints “B” and “C” of the tunnel was performed in order to identify the depth and position of the Omega Seal (Fig. 4(a-b)). The previous investigation carried out by Alani and Banks [4] identified the position of the seal clearly at joint “A” using a 2GHz GPR antenna. Thereby, surveys of joints “B” and “C” were carried out primarily to compare the results of the previous survey as well as to confirm the dimensions of the structural layers, in particular the depth of the Omega Seal from the surface of the roof of the tunnel. The reported previous results showed that the rebar spacing of the concrete cover at joint “B” was slightly wider than at joint “A” and, hence, the depth of penetration offered by the 900MHz antenna could be favourable. The survey conditions during the previous survey at joint “C” were not ideal and, therefore, it was deemed necessary to include this joint for further study.

7. Data acquisition

Joints “B” and “C” were surveyed according to the procedure indicated by Alani [30]. This “Method Statement and Risk Assessment” document clearly explains the survey methodology adopted along with details of the equipment and machinery required for the survey.

Overall, the survey lasted two days and was carried out during night hours following complete closure of the tunnel from 8.00 pm to 4.00 am, in order to avoid disrupting traffic.

The survey was performed by manoeuvring the radar antenna over the surface (roof) of the tunnel in a grid pattern, with 40 cm spacing between scans. One grid square mesh with a transversal axis (T axis) running parallel to the tunnel wall was created for the inspection of each joint, as it is shown in Fig. 5.

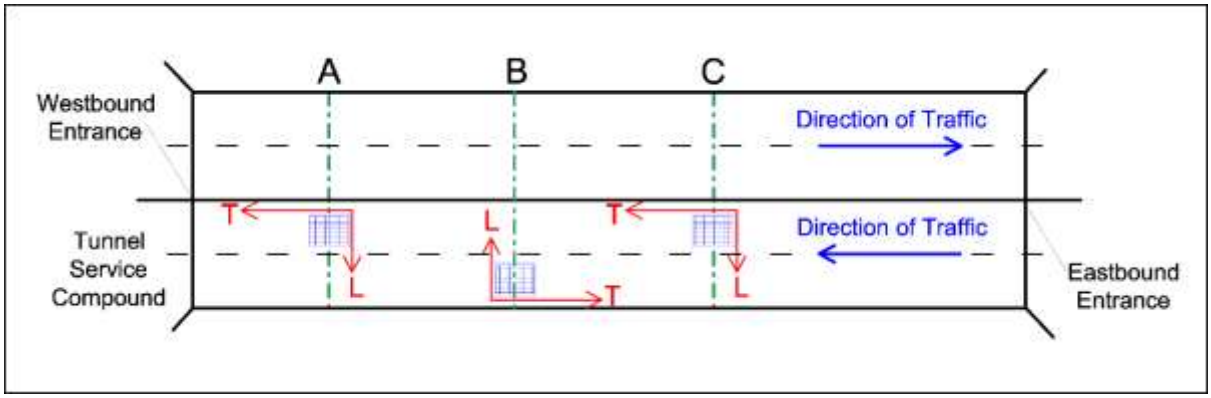

Fig. 5. Simplified drawing of survey grid locations.

As indicated in Fig. 6, the longitudinal axis (L axis) lined up with the outside edge of the clamp locations. As the roof of the tunnel is thicker closer to the walls than it is in the centre, and due to the dimensions and limitations of the survey platform used (i.e., a 6.00 m platform scissor lift), it was decided to start the survey 1.00 m away from the wall of the tunnel. In this case, moving/sliding the radar on the surface was achieved with ease. Similarly, one of the advantages of using a large platform was that the survey lines were covered without any interruption.

At the data collection stage, it was decided that no odometer would be used for the purposes of the survey to prevent difficulties caused by wheel slippage. These might have been caused by a layer of consolidated dirt/dust/particles covering the tunnel ceiling, which made it slippery to work on. A careful and steady speed of acquisition, along with a following processing of the data based on the use of position markers, allowed to relate the correct positioning to each acquired radar trace, which will be discussed later in this paper.

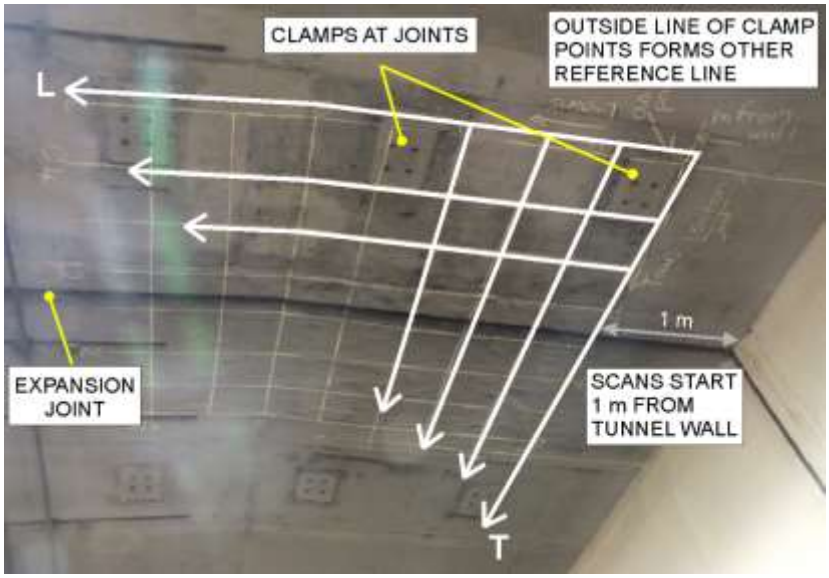

Fig. 6. Survey area and grid lines at joint “B”.

8. **Data Processing**

The IDS GRED HD3 software was used to process and interpret the collected data. To this intent, a processing scheme was run in order to enhance the useful information by limiting artifacts and lowering the clutter in the raw data. In particular, rubber-band interpolation, time-zero correction, band-pass filtering and smoothed gain were applied sequentially to the raw data.

A data acquisition mode implementing real-time stacking vertical processing allowed a reduction in the power level of uncorrelated noise. The use of markers has led to resampling the data in equally-spaced traces (rubber-band interpolation). Although the surveying speed was kept as constant as possible, a regular collection of radar traces in spatial terms would have been impossible to perform [31].

Horizontal processing was then applied. The time-zero was set at a common position, namely, the zero-amplitude point between the negative and the positive peaks. This reference point was chosen for ease of computing and the good stability along the surface of scanning [32].

A band-pass filter was applied to the signal considering a pass bandwidth of 1.5 times the central frequency of investigation with an even distribution of lower (high-pass filter) and upper (low-pass filter) boundaries around the central frequency [33, 34]. In more detail, a high-pass filter of 225 MHz and a low-pass filter of 1575 MHz were used to process the data collected with the 900 MHz frequency antenna system; whereas 500 MHz and 3500 MHz were set as high- and low-pass filters for the 2 GHz antenna, respectively. The application of this algorithm was aimed at increasing the signal-to-noise ratio (SNR) by filtering out the signal components with frequencies outside the main working bandwidth of the used GPR systems.

The use of the background removal allowed for a reduction in the clutter and the horizontal banding across the image by subtracting the average of all the GPR traces for each scan. The removal of the background noise enhances the subsurface reflections. It is important to emphasize that this filter is not effective in case of horizontal layers set as principal objective of the survey [33], whereas it is capable of emphasizing discontinuities or punctual objects in sub-horizontal concrete precast structures (i.e., joints or rebar layers in tunnel sections).

Finally, smoothed gain was applied to compensate for the attenuation suffered by the GPR signal when propagating through the medium, due to the dispersive nature of the EM waves and the geometrical spreading losses.

The velocity of the radar signal through the concrete was calibrated to fit the shape of the hyperbola which was found to be $v_{hyp.\ fitt}$ = 1.3 cm/ns within the joint. This process enabled the identification of features against the available design drawings.

Inside, the two joint layers of rebar were visible and then an interface; by using the hyperbola fitting function and guesstimating the shape of the hyperbola, it was possible to recognise that the velocity had increased significantly to $v_{hyp.\ fitt}$ = 25÷28 cm/ns (approximate because of the amount of guessing involved) and therefore it was possible to identify and confirm this as an

interface with a much less dense material containing a large proportion of air. This was consistent with the insulation layer.

9. Results and discussion

9.1. Joint “B”

Fig. 7 shows the survey grid adopted for the joint “B” survey. It can be seen that the transversal scans (scans across the joint) were acquired starting at 0.8 m, so that scans were only acquired across the immersion joint and one to either side. Previous surveys indicated that the data collected from outside these locations were not useful for the purposes of this study.

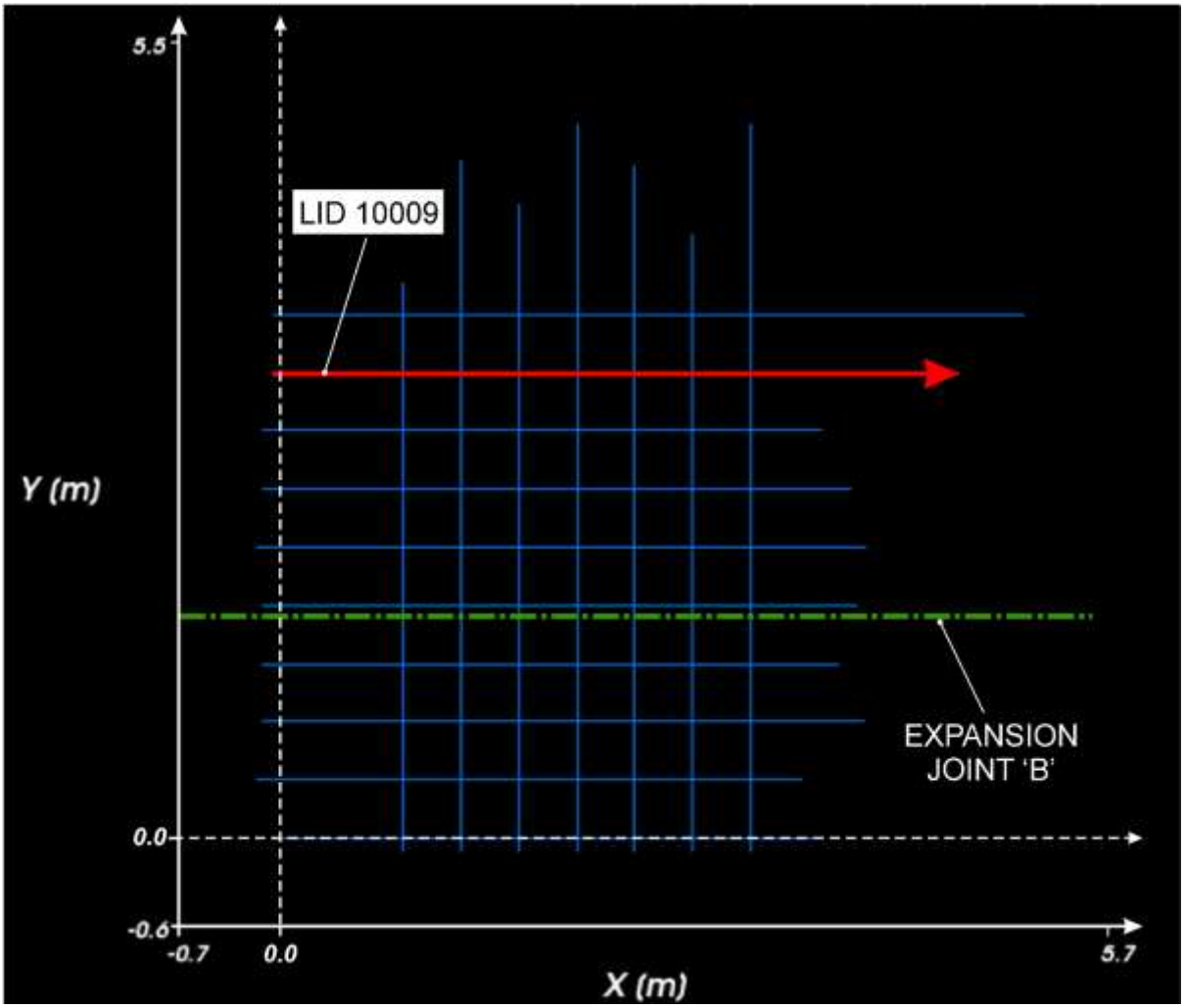

Fig. 7. Survey grid configurations at joint “B” (900 MHz antenna) with indication of the longitudinal scan LID10009 analysed in this study.

Fig. 8 and Fig. 9 depict the survey lines LID10009 (900MHz antenna) and LID10006 (2GHz antenna) respectively; it can be seen that similar features have been identified, including the presence of rebar layers and the location of the joint. However, there is the additional presence of an interface below the Rockwool Rollbats layer in Fig. 8 (data concerning the 900MHz antenna) that indicates a change in speed back to a level consistent with concrete. The higher resolution of the 2 GHz antenna allowed to identify depths of 12 cm and 27 cm for the first and second layer of rebar, respectively (Fig. 9), as well as to confirm the thickness of 41 cm for the shotcrete.

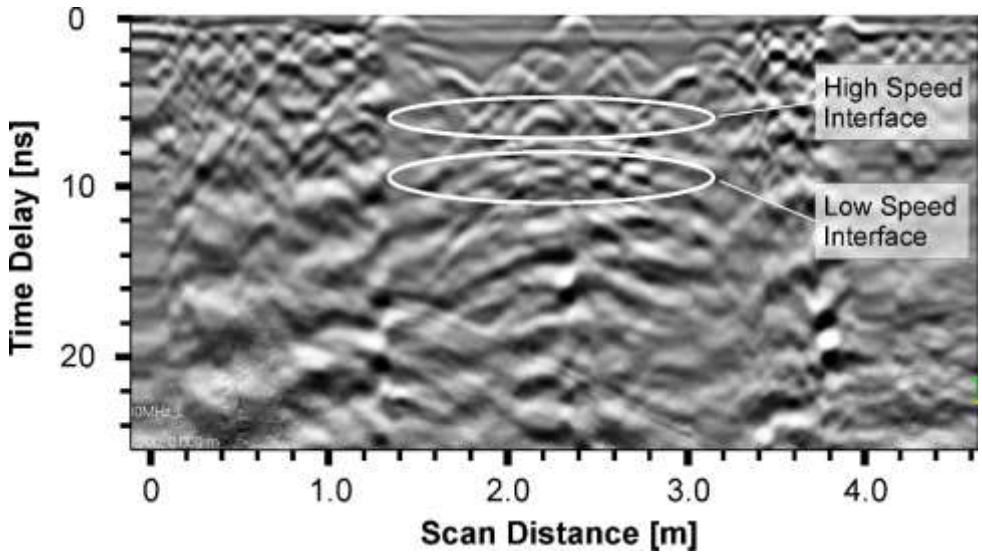

Fig. 8. Longitudinal scan (scan across the joint) LID10009 at joint “B” using 900MHz antenna.

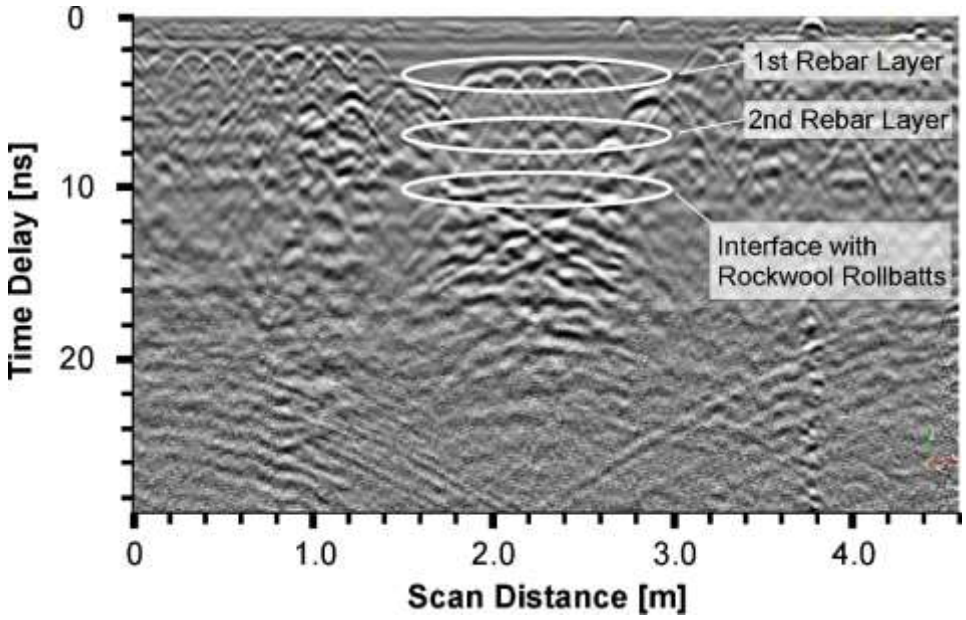

Fig. 9. Longitudinal scan LID 10006 at joint "B" using 2GHz antenna.

Fig. 10(a-c) depicts the identified features in velocity for the longitudinal scan of one of the surveyed lines (LID10009). Using the hyperbola fitting algorithm, the angle α between the two asymptotes *a* and *b* (Fig. 1(b)) was calculated. According to Eq. (7) and Eq. (8), it was then possible to estimate the velocity of propagation in the medium $v_{hyp.\,fitt}$ from the hyperbola fitting process and the depth of the target *D*, respectively.

A low speed $v_{hyp.\,fitt.}$ of 12.1 cm/ns before the interface of the Rockwool Rollbats was first detected (Fig. 10(a)), and used as a reference propagation speed for the time delay distance t_0 of 6.75 ns, identifying the depth of the interface related, possibly, to the lower part of the Omega Seal (Fig. 10(b)). A relevant depth of 82 cm was therefore assessed. Indeed, the hyperbola fitting algorithm in this time position returned a higher speed propagation value $v_{hyp.\,fitt.}$ = 27.5 cm/ns, which was taken as a reference for the thickness estimation of the Rockwool Rollbats layer. The relevant time position (t_0 = 8.75 ns) of the interface identifying the end of the Rockwool Rollbats layer (likely to be the Omega Seal) is indicated in Fig. 10(c). Hence, a relevant thickness of 55 cm for this layer was calculated as one of the main findings of this

work, apart from confirming the rebar layer depths and positions. This information was not achieved during the surveys with the higher frequency antenna system of 2GHz.

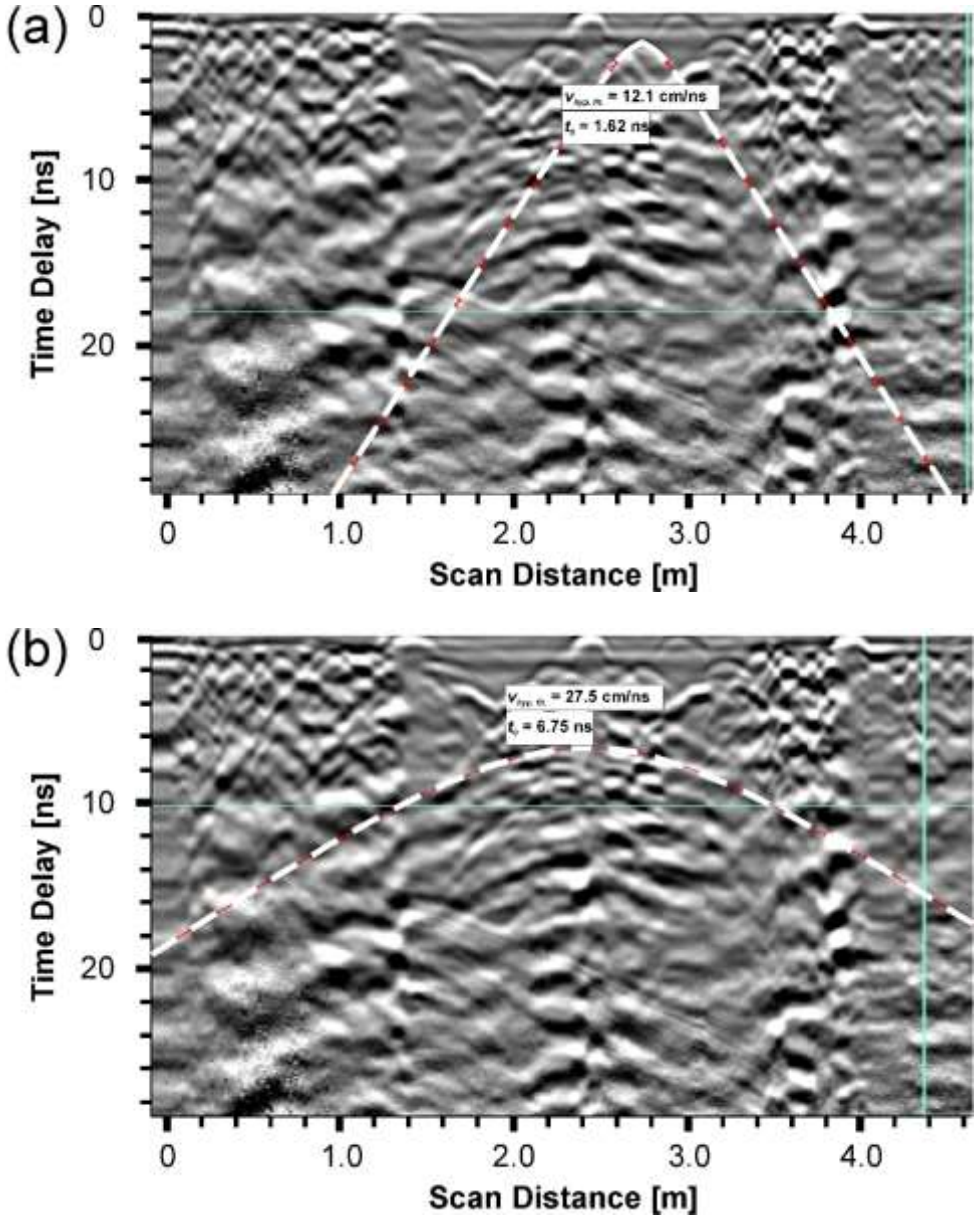

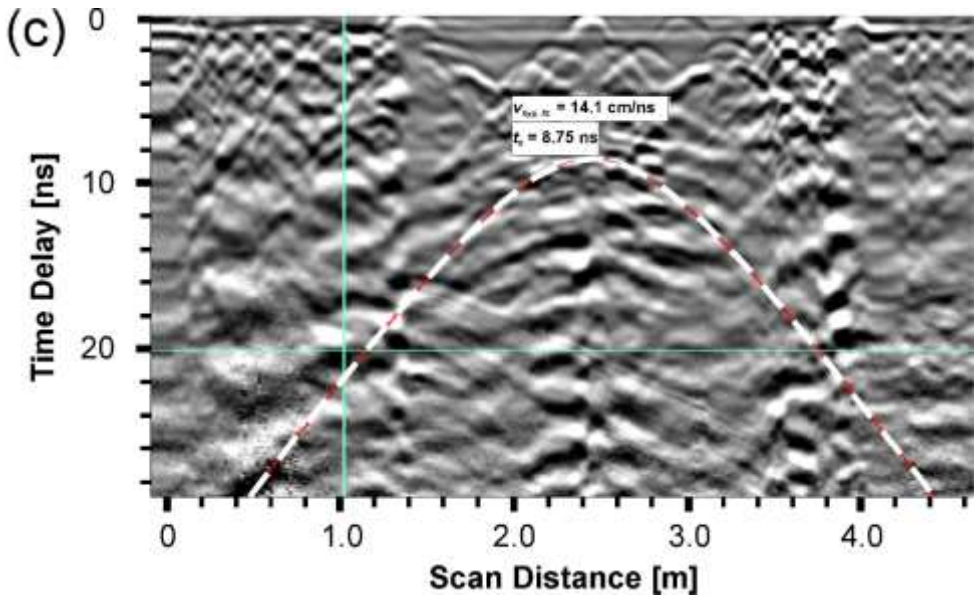

Fig. 10. Features identifying changes in velocity in the longitudinal scan LID10009 by hyperbola fitting, (a) low speed before the interface of the Rockwool Rollbats, (b) high speed interface identifying the depth of the lower part of the Omega Seal, (c) decreasing speed interface (end of the Rockwool Rollbats layer, likely to be the Omega Seal).

The results for joint "B" can be summarised as follows:

- Verification of results from previous survey (indicated in the drawing).
- Identification of Rockwool Rollbatts layer at 82 cm depth using the 900 MHz antenna. This was reported differently in the results of the previous surveys.
- Identification of the end of the Rockwool Rollbatts layer, likely to be the Omega Seal, at 137 cm depth using the 900 MHz antenna. This was reported differently in the results of previous surveys.
- With reference to Fig. 4(a-b) (original design drawings provided by the tunnel management team), the results of this survey reject the information provided by the design drawings in terms of dimensions as well as design details (two layers of rebar were identified which were not detailed in the design drawings provided). It was also identified that the concrete cover layer (shotcrete) which was originally reported as 25 cm is significantly out. The

survey results confirmed the presence of a minimum of 41 cm shotcrete at all the three immersion joints.

- Fig. 11 and Fig. 12 depict the construction details of the tunnel at joint “B” (3D and 2D cross-sections) based on the processed data obtained during this investigation. The data from the 900 MHz antenna confirmed the positions and configurations of the lower and upper rebar layers. In line with the higher resolution, a more accurate depth estimation was undertaken using the 2GHz antenna system. In addition, due to a relatively wider spacing of rebar at joint “B”, it was possible to penetrate more effectively beyond the two rebar layers. To that effect, a clearer estimation of the thickness of the Rockwool Rollbatts layer (55 cm) using the 900 MHz antenna became possible, according to the higher penetration of the radar system. This has been depicted in Fig. 11.

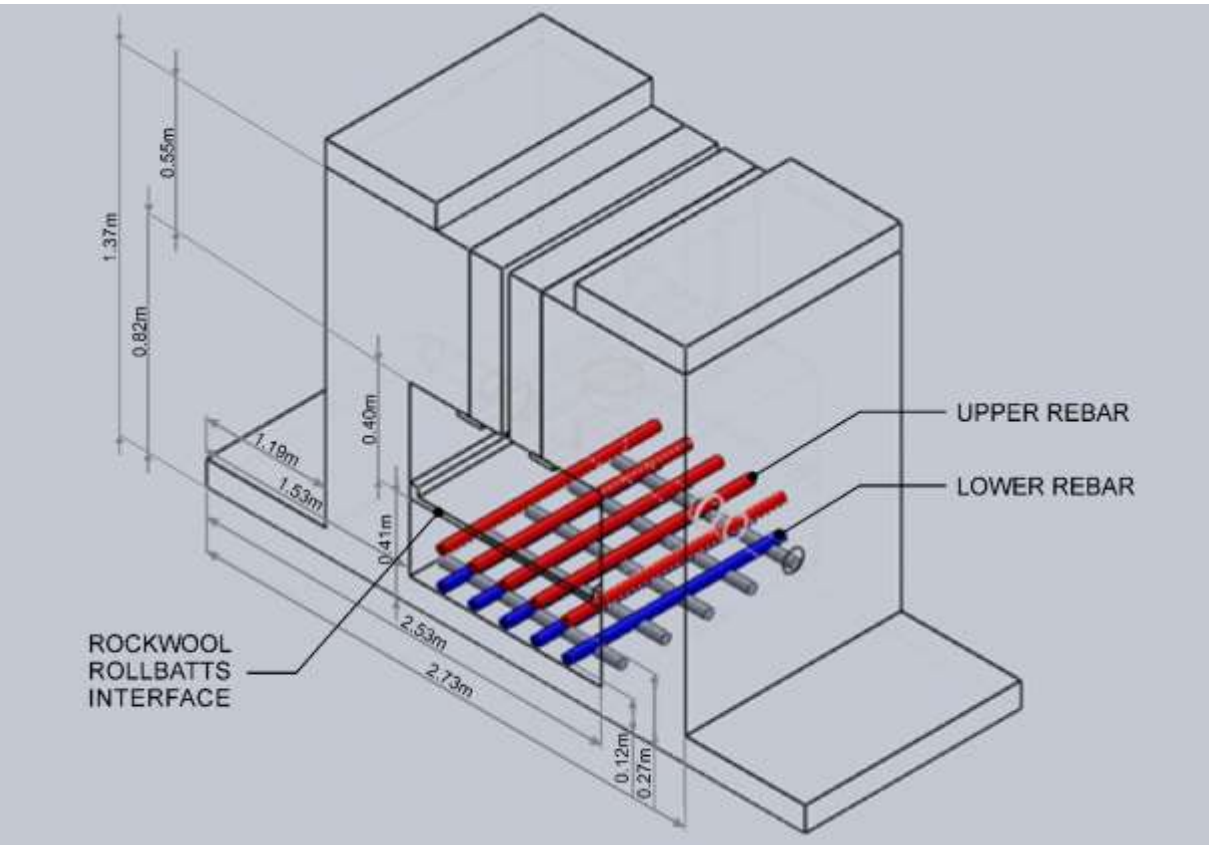

Fig. 11. 3D cross-section at joint “B” – actual construction details.

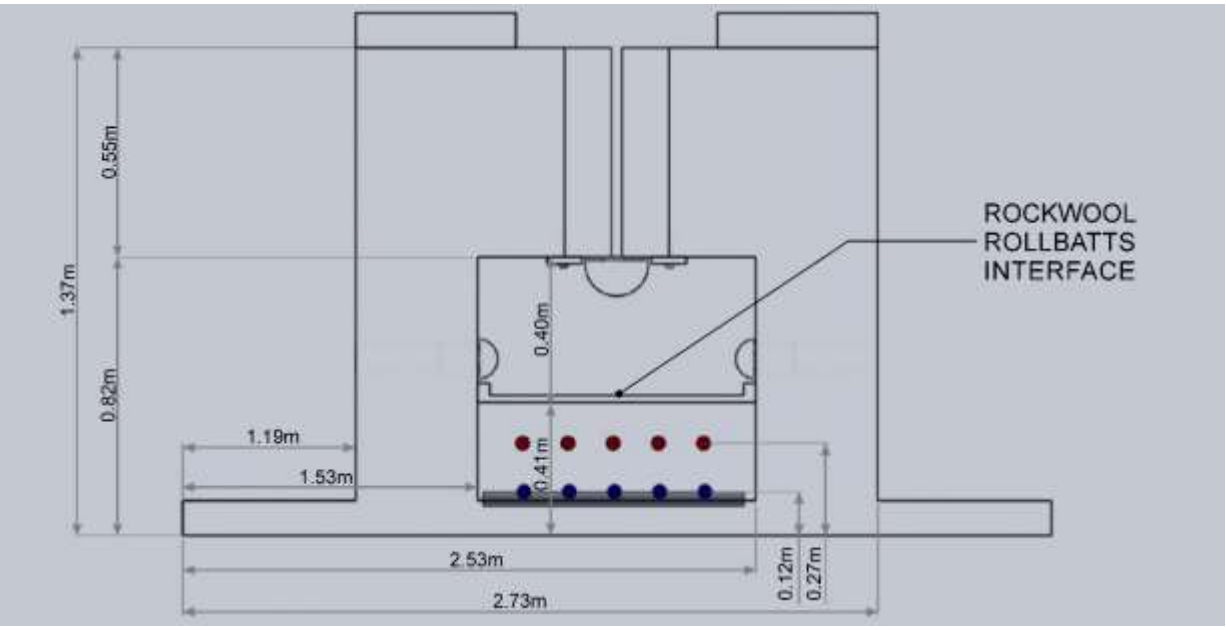

Fig. 12. 2D cross-section at joint “B” – actual construction details.

9.2. Joint “C”

Fig. 13 shows the survey grid for joint “C”. As explained earlier, due to the limitations of the 2GHz antenna in the penetration depth, it was deemed necessary to subject this joint to further investigations using a 900MHz antenna system. Fig. 13 indicates the transversal scans (scans across the joint) that were acquired starting at 0.8 m, so that scans were only carried out across the immersion joint with one extra line of survey to either side of the joint. The results of the previous survey indicated that it was not necessary to extend the acquisition of data beyond the joint.

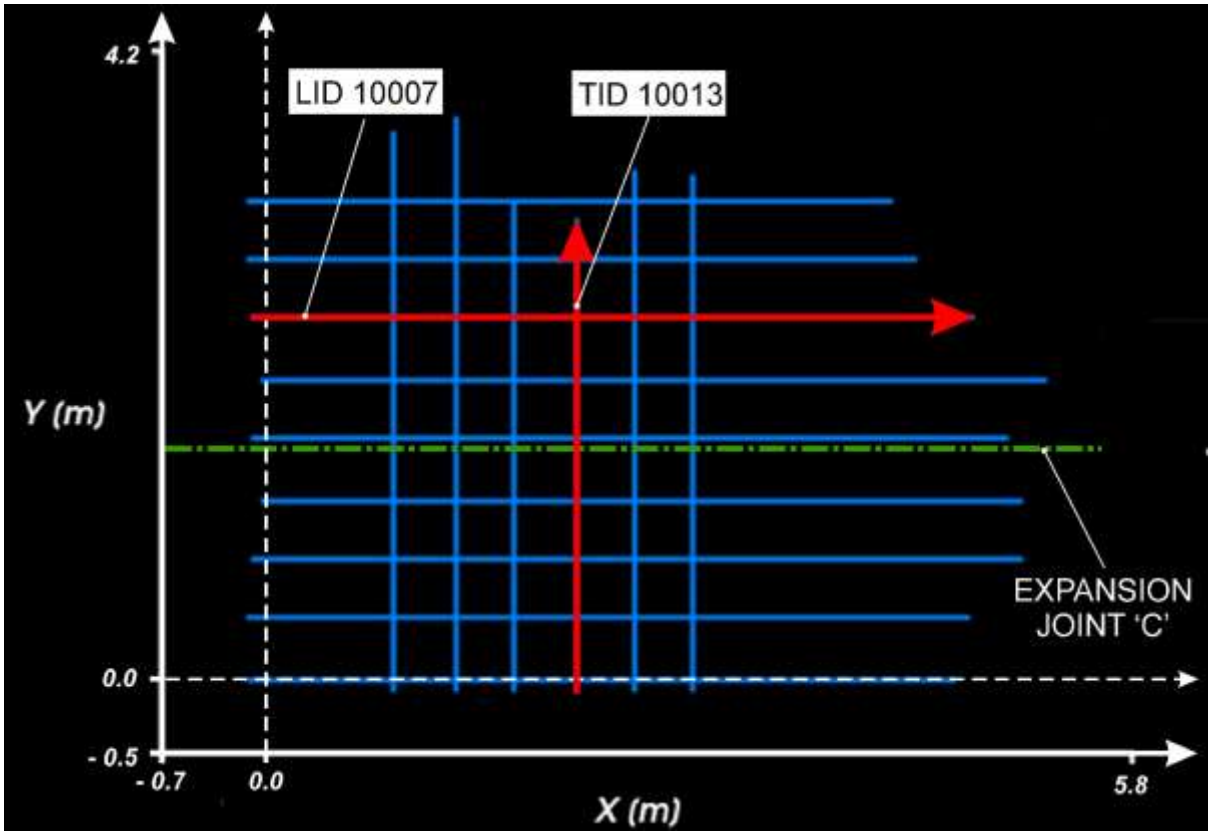

Fig. 13. Survey grid configurations at joint "C" (900 MHz antenna) with indication of the longitudinal scan LID10007 and transversal scan TID10013 analysed in this study.

The longitudinal scan LID10007 (across the immersion joint) verifies the results of the previous survey [4] and contains features consistent with a change in propagation speed which would identify the location of the immersion joint. This has been depicted in Fig. 14 and Fig. 15(a-c), which represent the results of some data processing as well as the velocity analysis carried out in terms of the identification of targets for the structural detailing of features at joint "C".

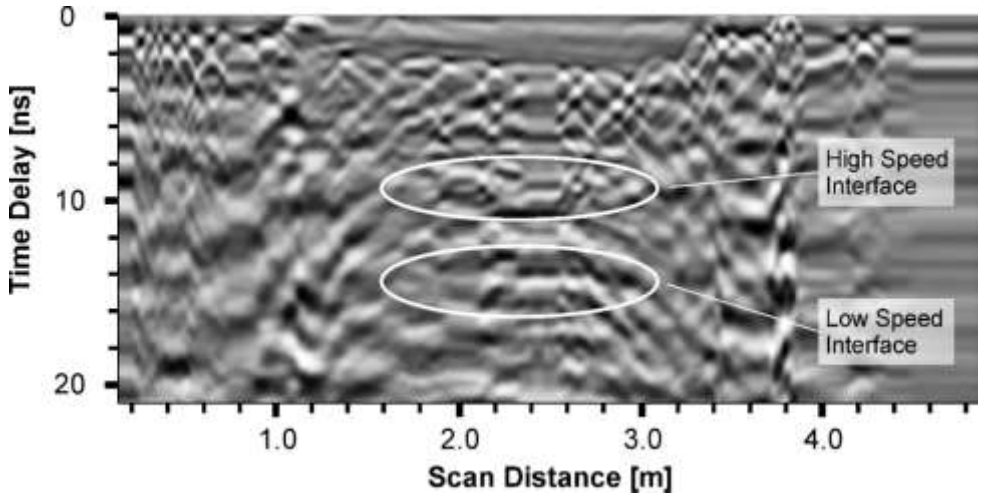

Fig. 14. Longitudinal scan LID10007 (scan across the joint) at joint "C".

The velocity analysis by hyperbola fitting provided useful information concerning the dimensions of the structural layers at the joint "C" position and, for the first time, it was possible to estimate the depth of the Omega Seal (lower part). Fig. 15(a-c) depicts the identified features for the longitudinal scan LID10007. Similarly to the case of joint "B", a low speed $v_{hyp.\ fitt.}$ = 15.1 cm/ns before the interface of the Rockwool Rollbats was first detected (Fig. 15(a)) and used for depth calculation across the time delay distance t_0 of 6.38 ns. This identified the depth of the interface possibly related to the lower part of the Omega Seal (Fig. 15(b)), that was found to be deep 95 cm. This information was vital to the tunnel owners as there had been no established dimensional information provided on this on the original design drawings. As in the case of joint "B", the velocity analysis returned a higher speed of propagation ($v_{hyp.\ fitt.}$ = 27.3 cm/ns), which was taken as a reference for the thickness estimation of the Rockwool Rollbats layer. The relevant time position t_0 of the interface identifying the end of the Rockwool Rollbats layer (likely to be the Omega Seal) was found to be 10.31 ns, as indicated in Fig. 15(c). Hence, a thickness of 109 cm was estimated for the Rockwool Rollbats layer.

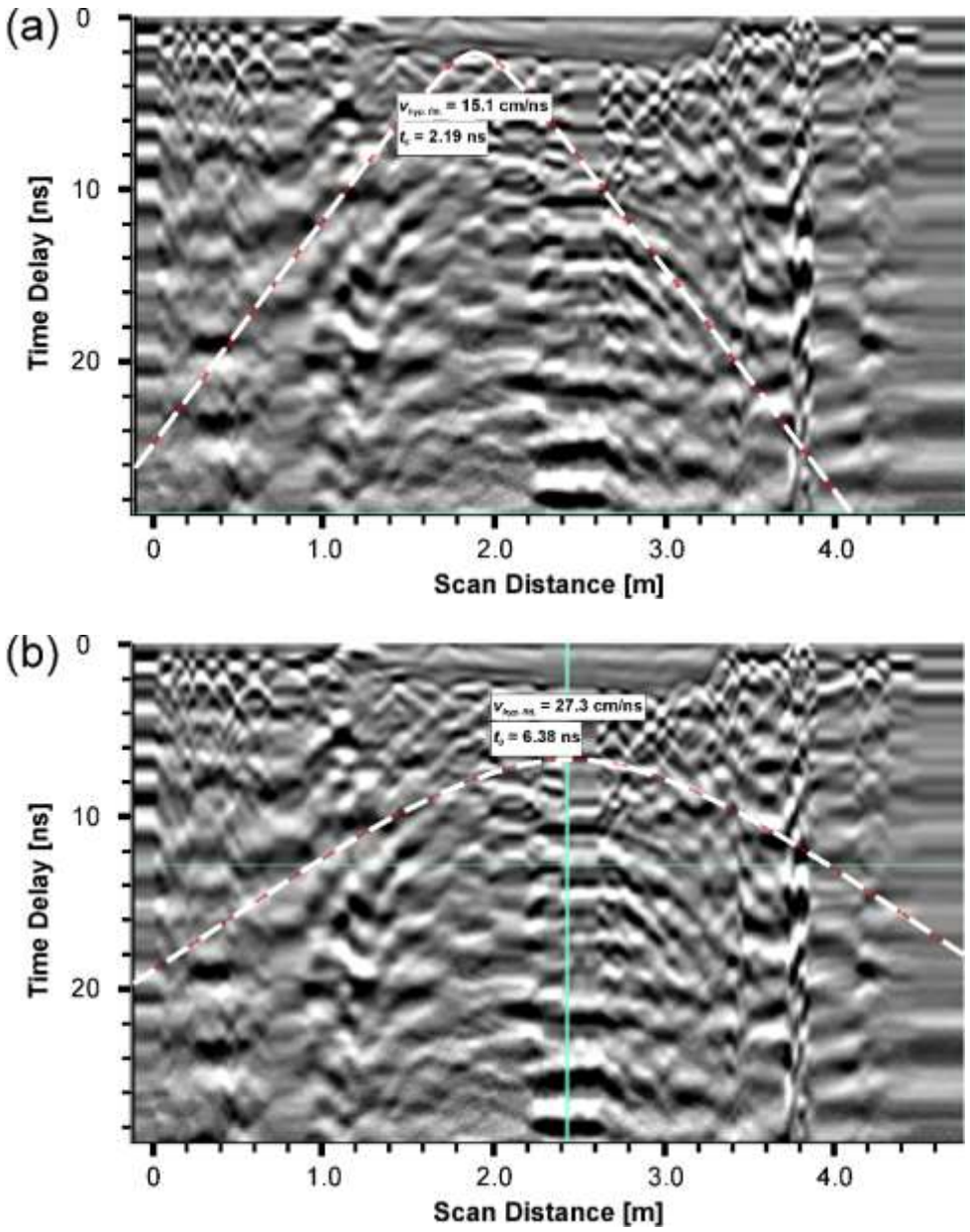
(a)
0
10
20
Time Delay [ns]
$v_{hyp.fix.}$ = 15.1 cm/ns
t_0 = 2.19 ns
0
1.0
2.0
3.0
4.0
Scan Distance [m]
(b)
0
10
20
Time Delay [ns]
$v_{hyp.fit}$ = 27.3 cm/ns
t_0 = 6.38 ns
0
1.0
2.0
3.0
4.0
Scan Distance [m]

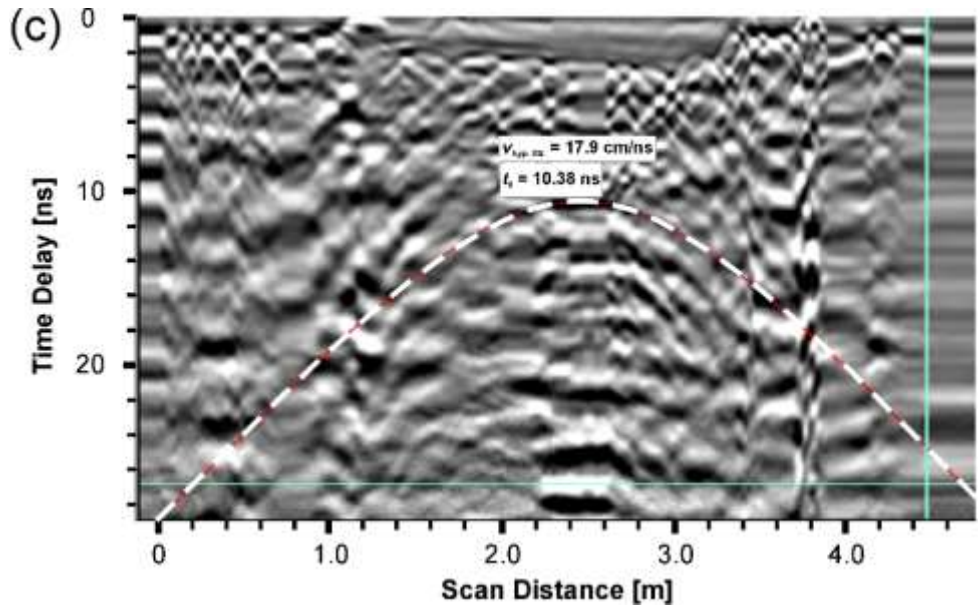

Fig. 15. Features identifying changes in velocity in the longitudinal scan LID10007 by hyperbola fitting, (a) low speed before the interface of the Rockwool Rollbats, (b) high speed interface identifying the depth of the lower part of the Omega Seal, (c) decreasing speed interface (end of the Rockwool Rollbats layer, possibly at the Omega Seal).

For the benefit of completeness, evidence of the data acquisition and processing of the transversal scanning carried out in this study is provided. Fig. 16 depicts the GPR data from a random scan along the joint “C”.

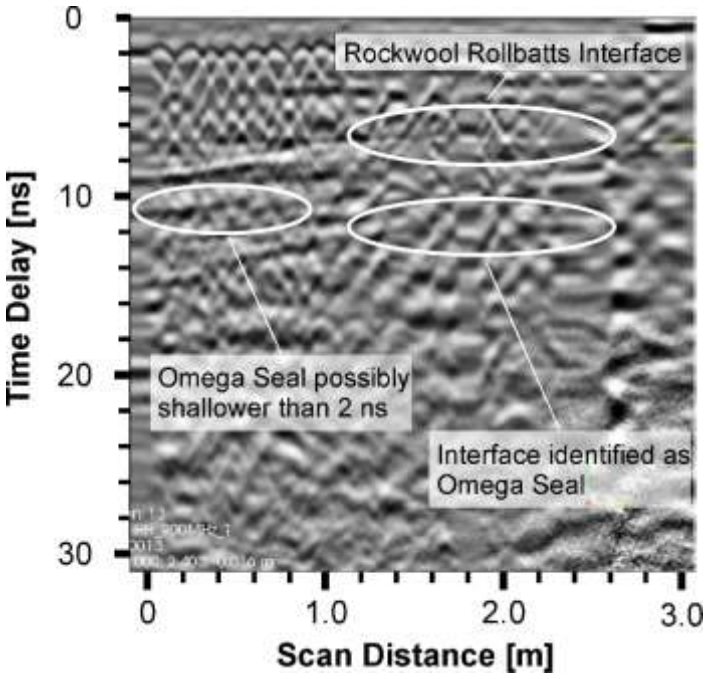

Fig. 16. Transversal scan of line TID10013 at joint "C" (scan along the joint).

The transversal scan above effectively verifies the data observed in the longitudinal scan. However, this scan identifies a new interface, not visible at the location of the scan using a 2GHz antenna, which is believed to be the Omega Seal. This would make the thickness of the Rockwool Rollbatts layer similar to joint "B"; however the correct interface cannot be 100% verified from the data obtained.

The higher resolution of the 2 GHz antenna allowed identification and provided details of shallower targets. Depths of 16 cm and 29 cm for the first and second layer of rebar, respectively (Fig. 9), were found, as well as the thickness of 40 cm for the shotcrete.

The results for joint "C" can be summarised as follows:

- Verification of results from previous survey (indicated in the drawing).

- Identification of Rockwool Rollbatts layer with the 900 MHz antenna system is estimated to be at 95 cm depth approximately. This is compatible with the results reported for joint "B".
- Identification of the end of the Rockwool Rollbatts layer, possibly at the Omega Seal, is estimated to be at 204 cm depth (see Fig. 17). It is reasonable to assume that this investigation depth was possible to reach due to the low electric conductivity and permittivity values of the mineral wool material [35] as well as to the large proportion of air in the composition of the Rockwool Rollbatts insulation layer. This is new and valuable information that was not achieved during the surveys with the 2 GHz antenna, due to the limitations of the frequency in the penetration depth.

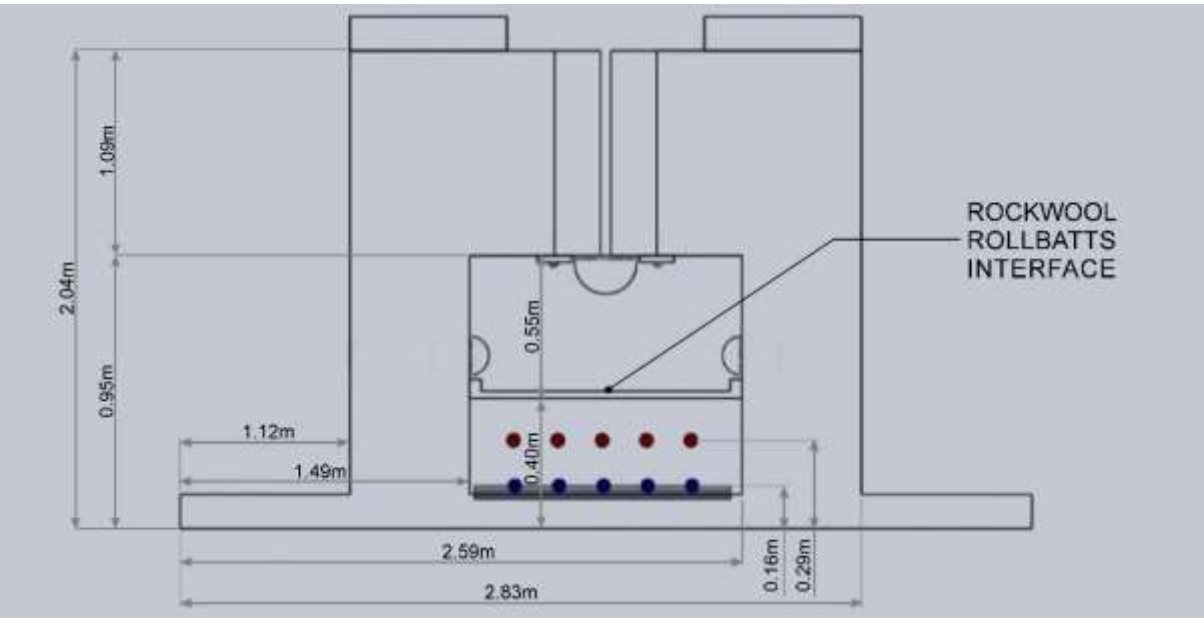

Fig. 17. 2D cross-section at joint "C" – actual construction details.

10. Conclusion and future prospects

This paper reports an extended study of applications of ground penetrating radar (GPR – 2GHz and 900MHz frequency antenna systems) on the structural detailing of a major tunnel located under the River Medway in north Kent, United Kingdom (the Medway Tunnel).

The lower resolution of the 900MHz antenna used in this investigation returned information of lower clarity in comparison to the 2GHz antenna survey. This is in regard to the interfaces identified of structural and functional elements across the joint. However, this study has confirmed that the same features are visible and can be considered as verified. This study has clearly demonstrated the benefit of using different GPR frequency antennas in achieving more accurate estimates of structural dimensions and features. This is particularly valuable when design information (drawings) are not available or when there are doubts about the construction details.

Both systems revealed the existence of two layers of rebar within the concrete cover layer, which were not known to exist from the available design drawings. Depth position and rebar spacing, as well as the thickness of the shortcrete were evaluated using the 2GHz GPR system. The 900MHz antenna system proved to be useful in providing information about the dimensions of the structural layers at the joint positions. This system also allowed an estimation of the depth of the Omega Seal (lower part). Although the depth of the GPR penetration has been blocked to a large extent by the previously mentioned two layers of rebar, it was possible to identify a change in pulse velocity at a depth of up to 200 cm approximately. The use of the hyperbola fitting algorithm for the estimation of the wave propagation velocity in composite materials, returned values in agreement with the theoretical expectations. In view of this, the investigation carried out in this study demonstrated the viability of GPR as a self-reliant non-destructive testing (NDT) method for the health monitoring of tunnel infrastructures as opposed to other non-intrusive inspection equipment used for the same purpose (e.g., the ultrasonic tomography (UST) and the impact echo (IE)). In addition, the amount and quality of the details

provided suggested a higher applicability to complex setups of data collection, such as in the case of structural detailing of the joints of an immersed tube tunnel, as proposed in this study. In fact, the possibility of obtaining two-dimensional scans with reliable depth dimensions, calibrated by avoiding intrusive methods (e.g., cores), makes the GPR a more comprehensive method of investigation. Furthermore, the research findings suggested that the use of multiple frequencies of investigation is recommended to obtain information about targets located at different depths with different shapes, dimensions and constituent materials.

Future research could task itself with focusing on calibration measurements of the Rockwool Rollbatts layer that may provide accurate indication of the propagation velocity through this material. This will result in improved depth measurements and structural detailing. Nevertheless, this study successfully confirmed that the interface which represents the Omega Seal (as per the as-built drawings) has been identified.

References

[1] ITA/AITES, Settlements induced by tunneling in soft ground, Tunnelling and Underground Space Technology, 22 (2007) 119–149.

[2] ITA/AITES, Report on the damaging effects of water on tunnels during their working life, Tunnelling and Underground Space Technology, 6 (1) (1991).

[3] L. Topczewski, F.M. Fernandes, P.J.S. Cruz, P.B. Lourenço, Verifying design plans and detecting deficiencies in concrete bridge using GPR, in Proc. of IABMAS'06, 3rd International Conference on Bridge Maintenance Safety and Management, Porto, Portugal, 2006.

[4] A.M. Alani, K. Banks, (2014), Applications of ground penetrating radar in Medway Tunnel – inspection of structural joints, in Proc. of the 15th International Conference on Ground Penetrating Radar (GPR 2014), Brussels, Belgium, Jun.-July 2014.

[5] J. White, S. Hurlebaus, P. Shokouhi, A. Wimsatt (2015), Nondestructive Testing Methods for Underwater Tunnel Linings: Practical application at Chesapeake channel tunnel, in Proc. of the International Symposium Non-Destructive Testing in Civil Engineering (NDT-CE), Berlin, Germany, Sept. 15–17, 2015.

[6] F. Lehmann, (2015). Practical application of non-destructive test methods at a single-shell tunnel lining, In Proc. of the 7th fib PhD Symposium in Stuttgart, Germany Sept. 11–13, 2008.

[7] A.G. Davis, M.K. Lim, C.G. Petersen, Rapid and economical evaluation of concrete tunnel linings with impulse response and impulse radar non-destructive methods, NDT & E Int., 38 (3) (2005) 181–186.

[8] O. Abraham, X. Dérobert, Non-destructive testing of fired tunnel walls: the Mont-Blanc Tunnel case study, NDT&E Int. 36 (2003) 411–418.

[9] E. Cardarelli, C. Marrone, L. Orlando, Evaluation of tunnel stability using integrated geophysical methods, J. Appl. Geophys., 52 (2003) 93–102.

[10] J. Hugenschmidt, Concrete bridge inspection with a mobile GPR system, Constr. Build. Mater., 16 (3) (2002) 147–154.

[11] H.-z. Yu, Y.-f. Ouyang, H. Chen, (2012), Application of Ground Penetrating Radar to Inspect the Metro Tunnel, In Proc. of the 14th International Conference on Ground Penetrating Radar (GPR), June 4-8, Shanghai, China.

[12] A.M. Alani, M. Aboutalebi, G. Kilic, (2013) Applications of Ground Penetrating Radar (GPR) in Bridge Deck Monitoring and Assessment, J. Appl. Geophys. 97 (2013) 45–54.

[13] F. Zhanga, X. Xie, H. Huang, (2010), Application of ground penetrating radar in grouting evaluation for shield tunnel construction, Tunn. Undergr. Sp. Tech. 25 (2010) 99–107.

[14] M-j Li, Y.-g. Zhao, H. Liu, Z. Wan, J.-c. Xu, X.-p. Xu, Y. Chen, W. Bin, Layer recognition and thickness evaluation of tunnel lining based on ground penetrating radar measurements, J. Appl. Geophys. 73(1) (2011) 45–48.

[15] L. Xiang, H.-l. Zhou, Z. Shu, S.-h.Tan, G.-q. Liang, J. Zhu, GPR evaluation of the Damaoshan highway tunnel: A case study, NDT&E Int. 59 (2013) 68–76.

[16] Q.-m. Yu, H.-l. Zhou, Y.-h. Wang, R.-x. Duan, Quality monitoring of metro grouting behind segment using ground penetrating radar, Constr. Build. Mater. 110 (2016) 189–200.

[17] X. Xie, C. Zeng, Non-destructive evaluation of shield tunnel condition using GPR and 3D laser scanning, in Proc. of the 14th International Conference on Ground Penetrating Radar (GPR), June 4-8, Shanghai, China, 2012.

[18] A. Wimsatt, J. White, C. Leung, T. Scullion, S. Hurlebaus, D. Zollinger, Z. Grasley, S. Nazarian, H. Azari, D. Yuan, P. Shokouhi, T. Saarenketo, Mapping voids, debonding, delaminations, moisture, and other defects behind or within tunnel linings. SHRP 2 Project R06-G, Prepublication draft. The second strategic highway research program 2, Washington, D.C.: Transportation Research Board of the National Academies; 2013.

[19] A. Benedetto, F. Benedetto, Remote sensing of soil moisture content by GPR signal processing in the frequency domain, IEEE Sensors J. 11 (10) (2011) 2432–2441.

[20] Z.-l. Huang, J. Zhang, Determination of parameters of subsurface layers using GPR spectral inversion method, IEEE T. Geosci.Remote 52 (12) (2014) 7527–7533.

[21] N.J. Cassidy, Electrical and magnetic properties of rocks, soils and fluids, in “Ground Penetrating Radar Theory and Applications” Ed. Jol, 41-72, 2008.

[22] S. Tillard, J.C. Dubois, Analysis of GPR data: wave propagation velocity determination, J. Appl. Geophys. 33 (1995) 77–91.

[23] S. Shihab, W. Al-Nuaimy, A. Eriksen. Radius estimation for subsurface cylindrical objects detected by ground penetrating radar. In Proc. of the 10th International Conference on Ground Penetrating Radar, Delft, The Netherlands, 2004 pp. 319-322.

[24] G. Borgioli, L. Capineri, P. Falorni, S. Matucci, C. Windsor, The detection of buried pipes from time-of-flight radar data, IEEE T. Geosci. Remote 46 (2008) 2254–2266.

[25] G. Olhoeft, Maximizing the information return from ground penetrating radar, J. Appl. Geophys. 43 (2000) 175–187.

[26] A. Dolgiy, A. Dolgiy, V. Zolotarev, 2006. Optimal radius estimation for subsurface pipes detected by ground penetrating radar. In Proc. of the 11th International Conference on Ground Penetrating Radar, Columbus, Ohio, USA.

[27] A. Ristic, D. Petrovacki, M. Govedarica, A new method to simultaneously estimate the radius of a cylindrical object and the wave propagation velocity from GPR data, Comput. Geosci. 35(8) (2009) 1620–1630.

[28] S. Shihab, W. Al-Nuaimy, Radius estimation for cylindrical objects detected by ground penetrating radar, Subsurf. Sens. Techn. Appl. 6 (2005) 151–166.

[29] G. Manacorda, A. Simi, M. Miniati, Mapping underground assets with fully innovative gpr hardware and software tools, In Proc. of The North American Society (NASTT) and the International Society for Trenchless Technology (ISTT) International No-Dig Show 2009, Toronto, Ontario Canada March 29 – April 3, 2009

[30] A.M. Alani, Method Statement and Risk Assessment document entitled: Medway Tunnel GPR and Laser Scanner Risk Assessment, Technical Report, 2014.

[31] G.R. Olhoeft, Maximizing the information return from ground penetrating radar, J. Appl. Geophys. 43 (2–4) (2000) 175–187.

[32] R. Yelf, D. Yelf, Where is true time zero? Electromagn. Phenom. 7 1 (18) (2006) 159–163.

[33] A. Benedetto, F. Tosti, L. Bianchini Ciampoli, F. D'Amico, (2016). An overview of ground-penetrating radar signal processing techniques for road inspections, Signal Process 132 (2017) 201-209.

[34] H. Jol, Ground Penetrating Radar: Theory and Applications, Elsevier, Amsterdam, The Netherlands, 2009.

[35] S. Xie, Y. Yang, G. Hou, J. Wang, Z. Ji, (2016). Development of layer structured wave absorbing mineral wool boards for indoor electromagnetic radiation protection, Journal of Building Engineering, 5, 79-85.